NJC

PAPER

View Article Online
View Journal | View Issue

Cite this: *New J. Chem.*, 2018, **42**, 6040

Photo-induced resonance energy transfer and nonlinear optical response in ball-type phthalocyanine conjugated to semiconductor and graphene quantum dots†

Njemuwa Nwaji, Ojodomo J. Achadu and Tebello Nyokong *

Received 31st December 2017,
Accepted 16th February 2018

DOI: 10.1039/c7nj05196d

rsc.li/njc

The synthesis of ball-type zinc and gallium phthalocyanines (complexes **2** and **3**) and their covalent linkage to glutathione (GSH) and amine functionalized quantum dots (QDs) are reported in this work. Furthermore, their photophysical, photo-induced resonance energy transfer and optical limiting responses were investigated. We observed a decrease in the fluorescence quantum yields with a corresponding increase in the triplet quantum yields of the nanoconjugates in comparison to the phthalocyanine complexes alone. The reverse saturable absorption was found to be dependent on the excited state absorption, and the observed limiting threshold ranged from 0.32 to 1.43 J cm^{-2}. Enhanced triplet parameters and nonlinear optical performance were found when the complexes were covalently linked to semiconductor quantum dots compared to carbon based graphene quantum dots.

Introduction

There has been a rising research interest aimed at designing materials that can afford a measure of protection to optical sensors and the human eye from hazards posed by intense laser radiation.[1–3] At reduced photonic energy, optical limiters exhibit linear transmittance but strongly attenuate optical beams to specific threshold levels under conditions of intense irradiation. Phthalocyanines (Pcs) have been known to exhibit large optical nonlinearities due to their extensive π-conjugated system and stability.[3,4] The strong reverse saturable absorption (RSA) behaviour of Pcs resulting from the enhanced excited state population makes these materials good candidates for optical limiting applications.

On the other hand, considerable attention has been paid to the use of nanomaterials in nonlinear optics (NLO) applications.[5–7] In particular, the nonlinear optical response of quantum dots (QDs) due to quantum confinement has been widely studied.[8–12] The dipole–dipole interactions of QDs (the donor) and phthalocyanine (the acceptor) may result in Förster resonance energy transfer (FRET) from the donor to the acceptor. FRET is generally employed to measure the molecular distance or donor-to-acceptor proximity.[13] The FRET-based enhancement of NLO response has been demonstrated in bacteriorhodopsin in the presence of QDs.[14]

It is expected that materials with an enhanced NLO response can be obtained from the synergistic interactions when QDs and optoelectronically active Pcs are combined. Indeed, improved optical limiting properties of phthalocyanine in the presence of semiconductor QDs (SQDs) have been reported.[15] Liu *et al.*[16] and Krishna *et al.*[17] reported significant improvement in NLO response of graphene quantum dots (GQDs) conjugated to porphyrins. The current work is the first report on the study of NLO behaviour of a ball-type phthalocyanine when linked to GQDs. Apart from our recent report,[18] the NLO study of ball-type phthalocyanine conjugated to SQDs has also not been reported. Phthalocyanines containing more than one ring such as bis-phthalocyanines are expected to show improved optical nonlinearities due to their expanded π electron system. This work reports on the NLO behaviour of the new 1′,11′,15′,25′-tetrakis[(carboxyphenoxy)bisphthalocyaninato]-zinc(II) (complex **2**) and gallium(III) (complex **3**) and compares them to the reported complex **4**[18] containing the same bridging ligands. We compare the effects of SQDs and GQDs on the NLO behaviour of complexes **2–4**.

Experimental

Materials

Zinc acetate, gallium chloride, absolute ethanol (EtOH), Rhodamine 6G, dicyclohexylcarbodiimide (DCC), 1-pentanol, 4-(dimethylamino)pyridine (DMAP), Zn phthalocyanine (ZnPc), 1,8-diazabicyclo[5.4.0]undec-7-ene (DBU), dimethyl sulphoxide (DMSO), and DMSO-d_6 were obtained from Sigma Aldrich®. Dimethylformamide (DMF), dichloromethane (DCM) and methanol were purchased

Department of Chemistry, Rhodes University, Grahamstown 6140, South Africa. E-mail: t.nyokong@ru.ac.za; Fax: +27 46 6225109; Tel: +27 46 6038260

† Electronic supplementary information (ESI) available: NMR spectra and MALDI-TOF mass spectra, absorption spectra, EDX spectra, XPS spectra, input *vs.* output plot, and biexponential decay curve of complex **6**. See DOI: 10.1039/c7nj05196d

from SAARCHEM®. Glutathione (GSH) capped CdTe semiconductor (SQDs)[19] and polyethyleneimine[20] functionalized graphene (GQDs) quantum dots were synthesized as reported in the literature. Synthesis of 3,4-bis(3,4-dicyanophenoxy)benzoic acid (**1**) has been reported previously.[18]

Equipment

Infrared spectra were measured using a Bruker® Alpha IR (100 FT-IR) spectrophotometer with universal attenuated total reflectance (ATR) sampling accessory. ^{1}H NMR spectra were recorded on Bruker® AVANCE II 400 MHz NMR spectrometers with tetramethylsilane (TMS) as an internal reference. Elemental analyses were carried out using a Vario-Elementar Microcube® ELIII while mass spectral data were collected on a Bruker® AutoFLEX III Smart-beam TOF/TOF mass spectrometer using a-cyano-4-hydrocinnamic acid as the matrix in the positive ion mode. The electronic ground state absorption spectra were recorded on a Shimadzu® UV-2550 spectrophotometer. Fluorescence excitation and emission measurements were carried out using a Varian Eclipse® spectrofluorimeter using a 360–1100 nm filter. The measurement of fluorescence lifetimes was carried out using a time correlated single photon counting setup (TCSPC) (FluoTime 300, Picoquant® GmbH) with a diode laser (LDH-P-670, Picoquant GmbH, 20 MHz repetition rate, 44 ps pulse width, where Pcs absorb). LDH-P-485 with 10 MHz repetition rate, 88 ps pulse width where QDs absorb.

The triplet decay kinetics were determined using a laser flash photolysis system. The excitation pulses were produced by a tunable laser system consisting of a Nd:YAG laser (355 nm, 135 mJ/4–6 ns), pumping an optical parametric oscillator (OPO, 30 mJ/3–5 ns) with a 420 to 2300 nm (NT-342B, Ekspla) wavelength range. Triplet lifetimes were determined by the exponential fitting of the kinetic curves using the ORIGIN® 8 Professional software. Transmission electron microscope (TEM) images were obtained using a Zeiss 1210 TEM operated at a 100 kV accelerating voltage. Energy dispersive X-ray spectroscopy (EDS) was performed using an INCA PENTA FET coupled to a VAGA TESCAM using a 20 kV accelerating voltage.

All the Z-scan measurements were performed using a frequency doubled Nd:YAG laser (Quanta-Ray, 1.5 J/10 ns fwhm pulse duration) as the excitation source. The laser was operated in a near Gaussian transverse mode at 532 nm (second harmonic). The liquid samples were placed in a cuvette (internal dimensions: 2 mm × 10 mm × 55 mm, 0.7 mL) and a path length of 2 mm (Starna 21-G-2).

Synthesis

Synthesis of 1′,11′,15′,25′-tetrakis[(carboxyphenoxy)bisphthalocyaninato] zinc(II) (2), Scheme 1. A mixture of zinc acetate (0.20 g, 1.09 mmol), 3,4-bis(3,4-dicyanophenoxy)benzoic acid (1, 0.25 g, 0.62 mmol), DBU (0.1 mL) and 1-pentanol (5 mL) was refluxed at 160 °C for 24 h under a nitrogen atmosphere. The product was precipitated out using methanol and collected through centrifugation. The product was washed with methanol, ethanol and 1 M HCl. The dark green product was further purified *via* reverse phase column chromatography using a dichloromethane and methanol (97 : 3) solvent mixture as the eluent. The purified product was dried in an enclosed fume hood. Yield: 0.18 g (45%), IR (ATR): ν (cm^{-1}): 3327 (OH stretch), 3108 (Ar–CH), 1562 (C═O stretch). ^{1}H NMR (400 MHz, DMSO-d$_6$) δ 10.35 (s, 4H, COOH), 8.24–8.13 (m, 14H, Ar–H), 8.08 (d, J = 8.0 Hz, 3H, Ar–H), 7.96 (d, J = 2.5 Hz, 3H, Ar–H), 7.60–7.53 (m, 7H, Ar–H), 7.48 (t, J = 7.6 Hz, 3H, Ar–H), 7.38 (d, J = 8.7 Hz, 6H, Ar–H). Anal. calc. for $C_{92}H_{40}Zn_2N_{16}O_{16}$, C, 62.92; H, 2.30; N, 12.76. Found: C, 63.74; H, 2.25; N, 12.91.

UV-vis, λ_{max}/nm (log ε): (DMSO), 688 (5.86), 620 (4.75), 361 (5.32). MALDI TOF-MS: calculated: 1756.22; found: 1757.38.

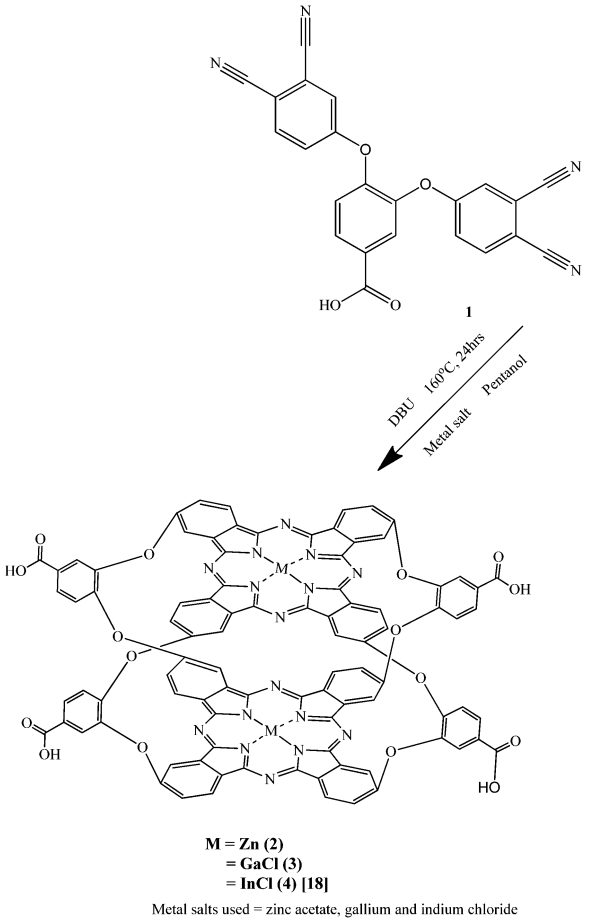

Scheme 1 Synthetic route for complexes **2** and **3**.

Synthesis of 1′,11′,15′,25′-tetrakis[(carboxyphenoxy)bisphthalocyaninato] gallium(III) chloride (3), Scheme 1. Complex **3** was synthesized as for **2** using gallium chloride (0.2 g, 1.10 mmol). Yield: 0.15 g (38%), IR (ATR): ν (cm^{-1}): 3276 (OH stretch), 2983 (Ar–CH), 1562 (C═O stretch). ^{1}H NMR (400 MHz, DMSO-d$_6$) δ 10.17 (s, 4H, COOH), 8.09–7.98 (m, 14H, Ar–H), 7.95 (d, J = 8.0 Hz, 3H, Ar–H), 7.83 (d, J = 2.5 Hz, 3H, Ar–H), 7.62–7.57 (m, 7H, Ar–H), 7.36 (t, J = 7.6 Hz, 3H, Ar–H), 7.14 (d, J = 8.7 Hz, 6H, Ar–H). Anal. calc. for $C_{92}H_{40}Cl_2Ga_2N_{16}O_{16}$, C, 60.19; H, 2.20; N, 12.21. Found: C, 61.03; H, 2.18; N, 12.37. UV-vis, λ_{max}/nm (log ε): (DMSO), 688 (5.12), 620 (4.35), 361 (4.98). MALDI TOF-MS: calculated: 1835.77; found: 1836.02.

Covalent linkage of SQDs and GQDs to complexes 2–4, Scheme 2. The conjugation was performed following a literature method.[18] Briefly, complexes **2** (0.025 g, 0.014 mmol),

3 (0.025 g, 0.014 mol), and **4** (0.025 g, 0.13 mol) were separately dissolved in 10 mL of DMF, followed by the addition of DCC (0.015 g, 0.072 mmol) to activate the carboxylic acid functional group. The reaction mixture was allowed to stir for 48 h at ambient temperature. After this time, DMAP (0.025 g, 0.082 mmol) and 0.01 g of SQDs or GQDs were added and the reaction was allowed to stir for a further 48 h at ambient temperature. The formed nanoconjugates were precipitated out of solution with methanol and collected through centrifugation, washed several times using ethanol and dried in an enclosed fume hood. The nanoconjugates are represented as **2**-GQDs, **3**-GQDs, **4**-GQDs, **2**-SQDs, **3**-SQDs, and **4**-SQDs.

Fluorescence and triplet quantum yields

The fluorescence (Φ_F) and triplet (Φ_T) quantum yields were determined using the comparative methods as reported in the literature,[21–23] using ZnPc as a standard (Φ_F = 0.20,[22] when exciting at absorption wavelengths of the Pcs) and Φ_T = 0.65[23] in DMSO. Rhodamine 6G dissolved in ethanol was used as a reference standard (Φ_F = 0.95,[24]) for QDs in a phosphate buffer solution (PBS) when exciting where QDs absorb (400 nm for SQDs and 320 nm for GQDs). The fluorescence quantum yields are represented as $\Phi_{F(Pc)}$ for excitation where the Pc absorbs and as $\Phi_{F(QDs)}$ when exciting where QDs absorb. Eqn (1) was used to determine the fluorescence quantum yields of the QDs following the covalent linkage of complexes **2–4** ($\Phi_{F(Pc-QDs)}$)

$$\Phi_{(Pc-QDs)} = \Phi_{F_{(QDs)}} \frac{F_{(Pc-QDs)}}{F_{QDs}} \quad (1)$$

where $F_{(Pc-QDs)}$ and F_{QDs} are the fluorescence intensities of QDs in Pc–QDs conjugates and QDs alone, respectively. $\Phi_{F(QDS)}$ represents the fluorescence quantum yield of the QDs alone and was used as a standard.

Results and discussion

Synthesis and characterization of the complexes and the nanoconjugates

The synthesis of the binuclear ball-type complex **4** (containing In central metal) has been reported,[18] and the synthesis of **2** and **3** followed the same procedure through cyclotetramerization of 4-bis(3,4-dicyanophenoxy)benzoic acid (**1**) using catalytic amounts of DBU and 1-pentanol as the solvent (Scheme 1). The formation of **2** and **3** was confirmed by the disappearance of the CN peak observed at 2230 cm^{-1} in the FT-IR spectrum of **1**. The structure and purity of the complexes were further confirmed using UV-vis, ^{1}H NMR, IR, mass spectra data and elemental analyses which agreed with the proposed structure.

^{1}H NMR spectra for complexes **2** and **3** showed the proton of the carboxylic acid at 10.35 and 10.17 ppm, respectively, which integrated into a total of 4 protons for each (Fig. S1, ESI,† using complex **2** as an example). The aromatic protons appear at 8.24–7.38 ppm for **2** and 8.09–7.14 ppm for **3** and integrated to give an anticipated number of 36 protons.

Fig. S2 (ESI†) shows the MALDI-TOF mass spectra of the complexes and the simulated mass fragments when isotopic mass distribution is considered. Variability in the relative abundance of the monoisotopic peak is expected due to an increased probability for multiple heavy isotopes as the mass of a molecule increases; hence the isotopic distribution model has been shown to be an accurate method of assigning molecular mass in large molecules[25] such as the one employed in this work. The observed experimental mass of the complexes was in good agreement with the calculated one.

The amide linkage route (Scheme 2) was employed for the covalent linkage of **2** and **3** to QDs using DCC to activate the carboxylic acid group and DMAP for coupling.

Optical spectroscopy

Electronic absorption spectra of complexes **2** and **3** as well as the quantum dots alone and when covalently linked are shown in Fig. 1 (**2**-GQDs and **3**-SQDs as representatives). Complexes **2** and **3** showed a monomeric behavior with single intense Q bands, typical of metalated Pc with degenerate D_{4h} symmetry.[26] The Q band maxima of complexes **3** and **4** are at 689 nm and 695 nm, respectively, more red-shifted compared to 682 nm observed for complex **2**, Table 1.

Red shifts in the Q band are typical for MPcs containing central metals with big atomic radius in the Pc cavity[27] due to a decrease in the energy gap between the highest occupied molecular orbital (HOMO) and the lowest unoccupied molecular orbital (LUMO).

Splitting of orbitals and lowering of the symmetry is expected to result in splitting or broadening of the Q band in ball-type Pcs due to the strong intermolecular interaction between the Pc rings.[28,29] There is no clear splitting of the Q band for complexes **2** and **3** in Fig. 1. Non-splitting of the Q band in ball-type Pcs is expected with dimers having eclipsed rather than staggered conformations.[30] The lack of splitting in the Q band has also been observed in other ball-type Pcs.[31] The absorption maxima for GQDs and SQDs before conjugation were found to be 348 nm and 537 nm, respectively, in DMSO (Table 1).

Upon covalent linkage of **2**, **3** and **4** to QDs, the absorption maxima for the GQDs were found to be 352 nm, 358 nm, and 356 for **2**-GQDs, **3**-GQDs, and **4**-GQDs, respectively (Fig. 1A, using **3**-GQDs as an example). The SQDs exhibit the absorption maxima at 561 nm, 565 nm, and 567 nm for **2**-SQDs, **3**-SQDs, and **4**-GQDs, respectively (Fig. 1B, using **3**-SQDs as an example, Table 1). There are red shifts in the absorption bands of both types of QDs following linkage to Pcs due to aggregation.

The emission spectra of complexes **2**, **3** and **4** are mirror images of both the absorption and excitation (Fig. S3A, ESI,† using **2** as an example). It can be observed that the absorption and excitation spectra are close, indicating that the nuclear configuration of the complexes was not affected at 615 nm excitation wavelength. A similar trend was also recorded following covalent linkage of the Pc complexes to QDs (Fig. S3B, ESI,† using **3**-SQDs as an example).

There is a high probability of more than one Pc molecule being attached to the nanoparticles since the approximate size of Pc (1 nm) is far less than that of the nanoparticles (>5 nm, Table 1 and discussed below under TEM). The loading of

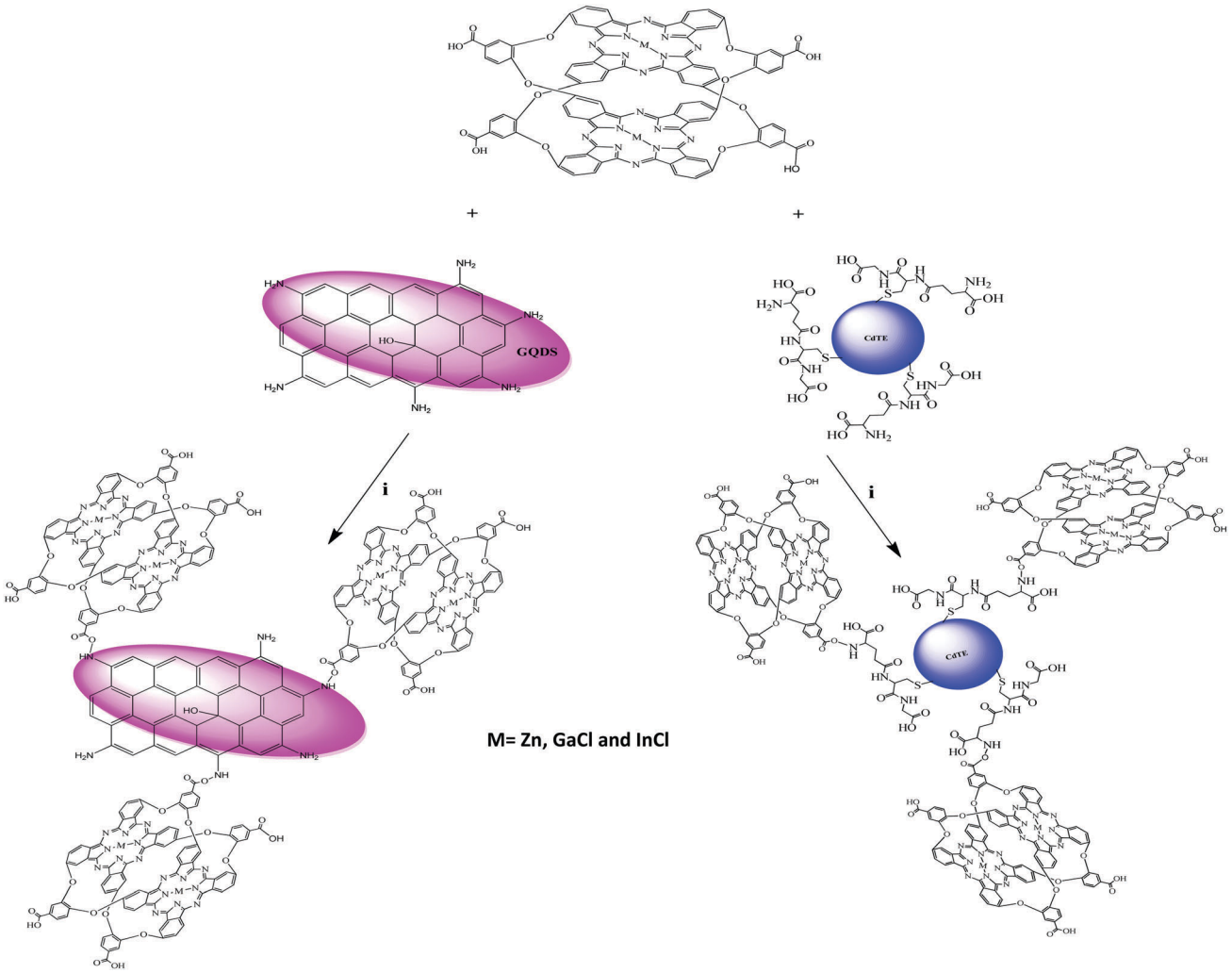

Scheme 2 Illustration of the synthetic route for covalent linkage of the phthalocyanine complexes to quantum dots.

complexes onto the nanoparticles was investigated following a literature report[32] but using absorption instead of fluorescence. This involves comparing the Q band absorbance intensity of equivalent weight of the Pc conjugate with that of the initial Pc before the conjugation and using the Beer–lambert relationship to determine the ratio of Pcs per nanoparticle. The estimated loading showed the number of Pcs per nanoparticles ranging from 7 to 15 (Table 1). It was observed that a higher number of Pc were loaded in the GQD conjugates than the corresponding SQDs except for complex **4**.

Generally, free carrier absorption is believed to be the dominant mechanism of nonlinear response in quantum dots, especially the semiconductor quantum dots[33,34] due to quantum confinement. Free carrier absorption occurs when a material absorbs a photon, resulting in excitation of a carrier (electron or hole) from an already-excited state to another unoccupied state. For free carrier absorption (FCA) to occur, the fundamental energy gap in the nanocrystals must be less than 4 eV,[35] which will lead to thermal excitation of an electron from the valance band (VB) to the conduction band (CB) due to the influence of external perturbation such as absorption of photon energy. The absorption spectra of quantum dots, which arise from excitation of electrons from the VB to CB, can be used to obtain the nature as well as the value of the effective optical band gap. Fig. S4 (ESI†) shows the Tauc plots derived from the absorption coefficients of the nanoparticles. The effective band gap E_g^{eff}(QD) was found to be 0.48 eV and 1.62 eV for GQDs and SQDs, respectively, thus FCA is expected for both GQDs and SQDs in this work. The size of the nanoparticles can be calculated with a known effective band gap using the Brus eqn (2).[35]

$$E_g^{eff}(\mathrm{QDs}) = E_g(\mathrm{bulk}) + \frac{h^2\pi^2}{2\mu R^2} \quad (2)$$

where R is the particle radius, E_g(bulk) is the bulk band gap energy (1.5 eV for CdTe SQDs[36] and 0.0 eV for GQDs[37]), h is the Planck's constant, E_g^{eff} is the effective band gap energy and μ is the effective reduced mass, which is given by eqn (3).

$$\frac{1}{\mu} = \frac{1}{M_e^*} + \frac{1}{M_h^*} \quad (3)$$

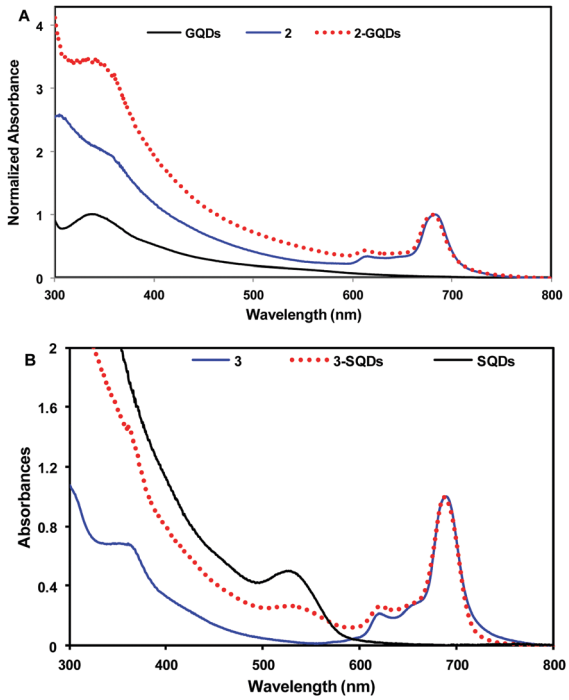

Fig. 1 UV-vis absorption spectra of quantum dots and the complexes alone and when covalently linked. Solvent: DMSO.

where M_e* and M_h* are the effective mass of the excited electron and hole respectively, and have been found to be 0.2 and 0.6, respectively, for QDs.[38] Substituting eqn (3) into 2 yields 4

$$E_g^{eff}(\text{QDs}) = E_g(\text{bulk}) + \frac{h^2\pi^2}{2R^2}\left[\frac{1}{M_e^*} + \frac{1}{M_h^*}\right] \quad (4)$$

The diameters of the QDs were estimated from the radii and found to be 5.0 nm and 8.6 nm, for GQDs and SQDs, respectively. Thus, SQDs are larger in size than GQDs.

TEM Images and DLS size determination

Monodispersed particles were observed in the TEM micrographs of the GQDs and SQDs with an average size of 5.9 nm and 9.6 nm, respectively, Table 1, which is in good agreement with the theoretically calculated sizes using the Brus model.

After linkage of **2**, **3** and **4** to GQDs, increases in size to 9.3 nm, 8.7 nm and 7.2 nm were observed for **2**-GQDs, **3**-GQDs, and **4**-GQDs, respectively. Similarly, the size of **2**-SQDs, **3**-SQDs, and **4**-SQDs increased to 11.2 nm, 10.1 nm and 12.3 nm, respectively (Fig. 2 using GQDs, SQDs, **2**-GQDs and **3**-SQDs as examples). The increase in size could be attributed to the effect of aggregation following conjugation resulting from possible interaction between Pcs and the nanoparticles through π–π stacking.[26]

The DLS analysis also follows the same pattern with that of TEM. The sizes for GQDs and SQDs were found to be 7.05 nm and 9.80 nm, respectively, while the sizes for **2**-GQDs, **3**-GQDs, **2**-SQDs and **3**-SQDs were found to be 10.23 nm, 9.65 nm, 12.07 nm and 13.11 nm respectively (Fig. 3, using **2**-GQDs and **2**-SQDs as examples).

EDX, FTIR and Raman analysis

An energy dispersive X-ray spectrometer (EDX) was employed to qualitatively ascertain the elemental compositions of the nanoparticles before and after covalent linkage to Pcs. The EDX of the QDs alone showed the expected atoms. The sulphur in the GQDs is from sulphuric acid used to oxidize the graphene oxide precursor, while the chlorine in the SQDs alone comes from the

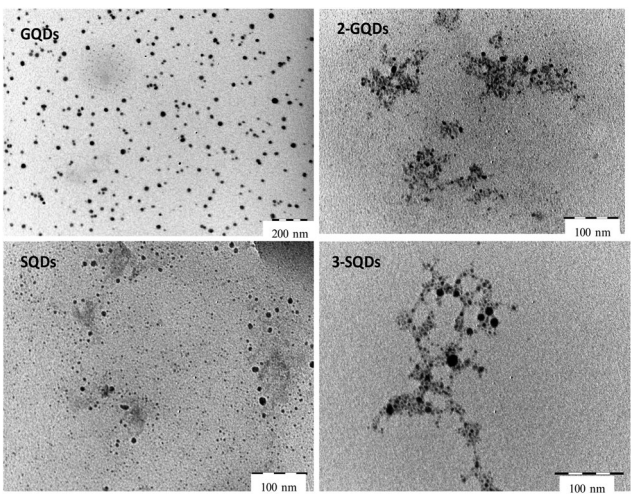

Fig. 2 TEM micrographs of quantum dots alone and when covalently linked to Pc complexes.

Table 1 Photophysical data of complexes **2–4** in the absence and presence of quantum dots in DMSO

Sample	Loading (Pc/NPs)	Size (nm) from TEM[a]	λ_{abs}[b] (nm)	$\Phi_{F(Pc)}$[c]	$\tau_{F(Pc)}$ (ns)	$\Phi_{F(QDs)}$[a,d]	$\tau_{F(QDs)}$[a] (ns)	$\Phi_{T(Pc)}$	$\tau_{T(Pc)}$ (μs)	τ_{ISC} (ns)
2	—	—	682	0.20	3.2	—	—	0.58	289	5.52
3	—	—	689	0.12	2.7	—	—	0.67	102	4.03
4	—	—	695	0.04	2.25			0.81	59	2.78
2-GQDs	12	9.3 (5.9)	682 (352)	0.16	2.9	0.85 (0.89)	9.1 (10.4)	0.61	221	4.75
2-SQDs	8	11.2 (9.6)	682 (561)	0.13	2.5	0.47 (0.63)	11.3 (18.5)	0.67	189	3.73
3-GQDs	15	8.7 (5.9)	689 (358)	0.10	2.4	0.82 (0.89)	8.7 (10.4)	0.69	93	3.48
3-SQDs	11	10.1 (9.6)	689 (565)	0.08	1.9	0.39 (0.63)	10.9 (18.5)	0.72	72	2.64
4-GQDs	7	7.2 (5.9)	697 (356)	0.04	2.18	0.8 (0.89)	9.3 (10.4)	0.85	56	2.56
4-SQDs	9	12.3 (9.6)	699 (567)	<0.01	1.54	0.37 (0.63)	8.8 (18.5)	0.90	48	1.71

[a] Numbers in brackets are for nanoparticles alone. [b] Values in brackets are the absorption of QDs when linked to Pcs. Absorption maxima for GQDs and SQDs alone are 348 nm and 537 nm, respectively. [c] Excitation at 615 nm where Pcs absorb. [d] Excitation at 400 nm for SQDS and 320 nm for GQDs.

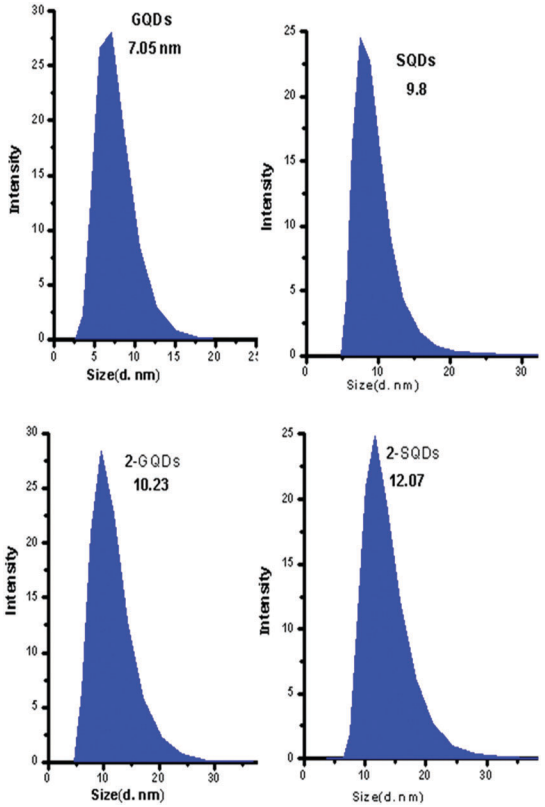

Fig. 3 Representative DLS graph showing average particle size for the nanoparticles alone and when covalently linked to **2**.

$CdCl_2$ starting material. Following conjugation of **2**, **3** and **4** to QDs, appearance of additional elemental peaks (Zn, Ga, In and Cl) confirms the presence of the complexes in the nanoconjugates (Fig. S5, ESI†) compared to QDs alone. The Cl is the axial ligand on the Ga and In central metals for the Pc.

The Raman spectrum obtained after conjugation of Pc complexes to GQDs displayed a shift in the characteristic D (disordered carbon atoms at the edges) and G (sp^2 bonded carbon atoms) bands of the GQDs (Fig. S6, ESI,† using complex **3** as an example). The observed Raman shift after conjugation is an indication of the introduction of defects within the carbon framework in the GQDs and confirmation of the formation of a new nanocomplex.

Fig. S7 (ESI†) (using complex **3** and the conjugates as examples) showed the FTIR of the Pc complexes, the QDs alone and when covalently linked. The carbonyl C═O stretches for complex **3** and GQDs were observed at 1562 cm^{-1} and 1498 cm^{-1}, respectively. Upon covalent linkage, a significant shift of the carbonyl peak to 1601 cm^{-1} corresponds to an amide bond (O═C–NH), suggesting successful linkage. A similar observation was recorded upon linkage to SQDs with the peak for the amide bond observed at 1616 cm^{-1} (Fig. S7, ESI†).

Forster resonance energy transfer (FRET) in the covalently linked conjugates

The Förster resonance energy transfer (FRET) is an important phenomenon for studying the energy transfer interactions between two molecules within several nanometers.[39,40] The mechanism of FRET involves a non-radiative energy transfer from a donor fluorophore in an excited electronic state to a nearby acceptor chromophore through long-range dipole–dipole interactions, resulting in the formation of a donor–acceptor pair. The rate of FRET generally shows strong dependence on the overlap between donor emission and acceptor. The normalized absorption spectra of complexes **2**, **3** and **4** as well as the photoluminescence spectra of the GQDs and SQDs are shown in Fig. 4.

The emission peaks of GQDs and SQDs were observed at 448 nm and 560 nm, respectively, under excitation at 320 nm for GQDs and 400 nm for SQDs. It can be seen from Fig. 4 that the absorption spectra of **2**, **3** and **4** overlap with the emission spectrum of the QDs. The overlap is weak for GQDs due to a blue shifted emission spectrum.

On excitation of the covalently linked nanocomposite at these wavelengths, a drastic quenching in the photoluminescence spectra of the SQDs was observed while the photoluminescence of the GQDs showed almost complete quenching with the emergence of a new peak between 620 and 750 nm for both nanoconjugates (Fig. S8, ESI†). This new peak is known as stimulated emission since it is not observed for the individual complexes using the same excitation wavelength and could be attributed to non-radiative energy transfer from the donor quantum dots to the acceptor Pcs. One dominant process that results in FRET for a donor–acceptor pair is the excited state quenching,[39] which can turn the ''bright'' QDs into ''dark'' QDs due to the attachment of the acceptor on the surface of the donor.

The FRET overlap function can be defined by eqn (5):[39]

$$J(\lambda) = \frac{\int_0^\infty F_D(\lambda)\varepsilon A\lambda^4 \partial\lambda}{\int_0^\infty F_D \partial\lambda} \quad (5)$$

where F_D is the normalized intensity of the QD emission spectrum and ε is the molar extinction coefficient (M^{-1} cm^{-1}) of the Pc. λ is the wavelength (nm) of the absorption maximum of the acceptor *i.e.* the Q-band. The efficiency of energy transfer can be experimentally determined using the fluorescence

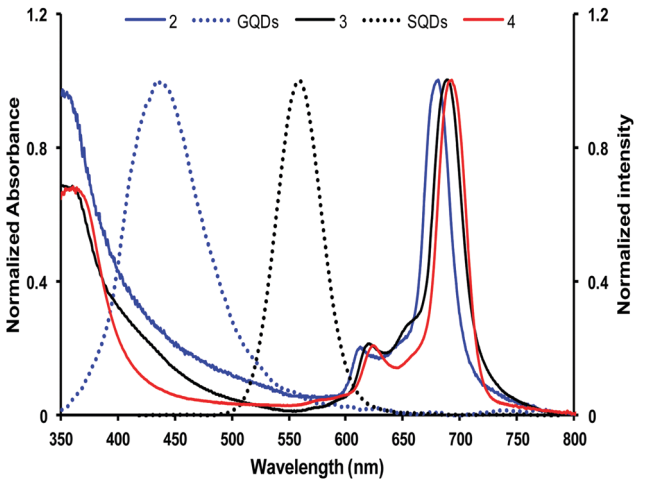

Fig. 4 Emission spectra (dotted line) of as-synthesized QDs and absorption spectra (solid lines) of **2–4** in DMSO.

quantum yield of the donor in the absence (Φ_{FDA}) and presence (Φ_{FDP}) of the acceptor using eqn (6) and (7).[39] The Förster distance, which is the critical distance between the donor and acceptor molecules at which the efficiency of energy transfer is 50%, is related to FRET efficiency by eqn (7) where r is the center to center distance between the donor and the acceptor.

The Förster distance, R_0 (Å) depends on the fluorescence quantum yield of the donor, eqn (8).

$$\text{Eff.} = 1 - \frac{\Phi_{FDP}}{\Phi_{FDA}} \quad (6)$$

$$\text{Eff.} = \frac{R_0{}^6}{R_0{}^6 + r^6} \quad (7)$$

$$R_0{}^6 = 8.8 \times 10^{23} k^2 n^{-4} \Phi_{FDA} J \quad (8)$$

where k is the dipole orientation factor (generally taken as 2/3 in a liquid medium since their dipole moments are considered to be isotropically oriented during the excited state lifetimes), n is the refractive index of the medium, Φ_{FDA} and Φ_{FDP} are the fluorescence quantum yield of the donor in the absence and presence of the acceptor, respectively, and J is the overlap function. FRET parameters were computed using the program PhotochemCAD[40] and presented in Table 2. The values of J were found to be 6.57×10^{13}, 1.27×10^{13}, 1.09×10^{13}, 5.70×10^{13}, 2.60×10^{14} and 2.27×10^{14} for **2**-GQDs, **3**-GQDs, **4**-GQDs **2**-SQDs, **3**-SQDs and **4**-SQDs, respectively (Table 2). In contrast, the corresponding FRET efficiencies were found to be 19.2%, 16.3%, 14.6%, 70.1%, 50.9% and 49.5%, respectively, suggesting a better transfer efficiency in semiconductor quantum dots compared to graphene based quantum dots due to better spectral overlap for the former.

Photophysical parameters

Time correlated single photon counting (TCSPC) was used to determine fluorescence lifetimes (τ_F). The decay curves of the QDs alone and in the presence of complexes **2** to **4** when exciting where QDs absorb are shown in Fig. 5 using **2**-GQDs and **3**-SQDs as examples.

A two-exponential decay was observed and fitted using eqn (9).

$$I(t) = \alpha_1 \exp(-t/\tau_0) + \alpha_1 \exp(-t/\tau_1) \quad (9)$$

where α is the normalization factor, $I(t)$ is the initial fluorescence at time t, and τ_0 and τ_1 are the different fluorescence lifetimes.

When exciting where SQDs absorb the average fluorescence lifetime ($\tau_{F(QDs)}$) was 18.5 ns in DMSO. The GQDs on the other hand showed a monoexponential decay with $\tau_{F(QDs)}$ = 10.4 ns in DMSO, Table 1. In the presence of Pc complexes, the $\tau_{F(QDs)}$ values decrease to 11.3 ns, 10.9 ns and 8.8 ns for **2**-SQDs, **3**-SQDs and **4**-SODs, respectively, Table 1. Similarly, the $\tau_{F(QDs)}$ values for **2**-GQDs, **3**-GQDs and **4**-GQDs were found to be 9.1 ns, 8.7 ns and 9.3 ns, respectively. All show a decrease in the presence of Pcs. A corresponding decrease in the fluorescence quantum yields was observed, Table 1. The decrease in both fluorescence quantum yields and lifetimes is the hallmark of FRET between the donor and acceptor molecules. On excitation at the absorption wavelength (615 nm) of complexes (**2–4**), a general decrease in fluorescence quantum yield (Φ_F) was observed in the conjugates compared to the MPc complexes alone, suggesting deactivation of the excited state singlet of the complexes by the nanoparticles through the external heavy atom effect for the SQDs, which promotes faster intersystem crossing. There was a smaller (or none) decrease in Φ_F for Pc conjugates bearing GQDs, which is expected due to the absence of heavy atoms in the nanoparticles. Expectedly, the fluorescence lifetimes (τ_F) also follow the same trend as the quantum yield since they have a direct relationship.

The triplet decay curve of the complexes (Fig. S9, ESI,† using complex **3** as an example) and the corresponding nanoconjugates showed second order decay kinetics, which is a well-known phenomenon for MPcs complexes at a high concentration, due to triplet–triplet recombination.[41] Generally, higher triplet

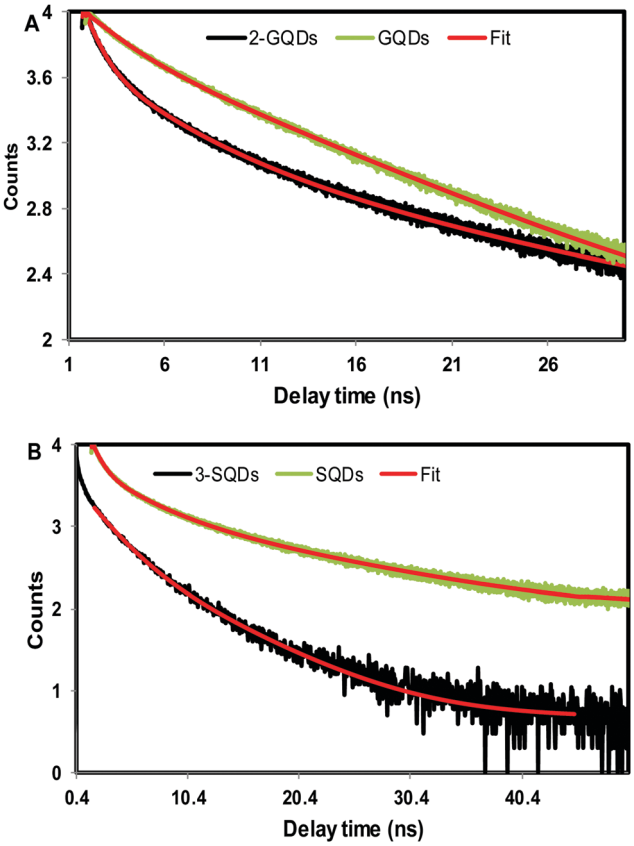

Fig. 5 Time resolved fluorescence decay curve of (A) GQDs and **2**-GQDs and (B) SQDs and **3**-SQDs. Fitted curve is shown in red. Solvent: DMSO.

Table 2 Energy transfer parameters for QDs–Pc conjugates in DMSO using the FRET method

Sample	J (λ) (M^{-1} cm^{-1} nm^4)	Eff. (%)	R_0 (Å)	r (Å)	k_T (r) (ns^{-1})
2-GQDs	6.57×10^{13}	19.2	64.5	92.7	0.012
3-GQDs	1.27×10^{13}	16.3	49.1	78.9	0.006
4-GQDs	1.09×10^{13}	14.6	41.3	73.5	0.014
2-SQDS	5.70×10^{13}	70.1	59.3	53.3	0.075
3-SQDs	2.60×10^{14}	50.9	40.2	38.7	0.039
4-SQDs	2.27×10^{14}	49.5	40.5	36.2	0.07

quantum yields were observed when the complexes were covalently linked to QDs with **4**-SQDs showing the highest triplet quantum yield of 0.90 compared to 0.81 for **4** before linkage (Table 1). The semiconductor quantum dots bearing complexes also showed enhanced triplet quantum yield compared with the graphene quantum dots bearing counterparts, which can be attributed to the presence of a heavy atom effect in the former compared to the latter. The increase in triplet quantum yield corresponds to the decrease in fluorescence quantum yield as expected since the two processes have an inverse relationship. There is a decrease in triplet lifetime with increase in triplet quantum yield as expected.

Nonlinear optical study

The nonlinear absorption response was investigated using the open aperture Z-scan technique at an excitation wavelength of 532 nm and 10 ns pulse duration using an input energy of 60 MW cm^{-2}. The Z-scan experiments were carried out for all the samples in solution using 1 mm quartz cuvettes. Prominent features of potential materials for optical limiting applications are possession of reverse saturable absorption (RSA).[3,42–44]

An RSA profile was observed in all cases for the complexes and the corresponding nanoconjugates, suggesting an induced positive nonlinear absorption of incident light intensity (Fig. 6 and Fig. S10, ESI†).

The linear transmittance for complex **2** was found to be 33%, lower than the 45% and 60% for **2**-GQDs and **2**-SQDs (Fig. 6A), respectively, which shows an enhanced nonlinear optical response following linkage of **2** to the QDs. Complex **3** showed a linear transmittance of 56%, and **4** showed 61%.

Transmittance values of 67% and 78% were observed for **3**-GQDs and **3**-SQDs, respectively (Fig. 6B). For **4**-GQDs and **4**-SODs, the values were 70% and 81%, respectively (Fig. S10, ESI†). Thus, in all cases the transmittance values for Pcs increased in the presence of QDs. It can be seen that complexes **3** and **4**, bearing Ga and In central metals, respectively, showed high RSA compared to complex **2** having a zinc central metal indicating the importance of the heavy atom effect in the NLO response. The conjugates bearing SQDs also showed enhanced RSA behaviors compared to the corresponding carbon based GQDs bearing conjugates due to the larger triplet quantum yields in the former. To understand the experimental results, the five-energy model (Fig. 7) was used to establish the population dynamics resulting from different states.

In the nanosecond regime, the five-energy model is vital since it can be used to estimate the singlet, the triplet, as well as the two-photon absorption (TPA), with the TPA-induced excited state absorption (ESA).[45–47] Based on this model, the nanosecond laser pulse at 532 nm will excite molecules from the ground state S_0 to either a first excited state (S_1) with ground state absorption cross-section of δ_0 through one-photon absorption or to a higher excited state (S_n) with an absorption cross-section δ_1. Molecules at the first excited state S_1 can radiatively decay to ground state S_0 with a decay lifetime τ_0. The population of the triplet state will be dependent on the rate of intersystem crossing and the triplet lifetime. The intersystem crossing lifetimes were calculated from

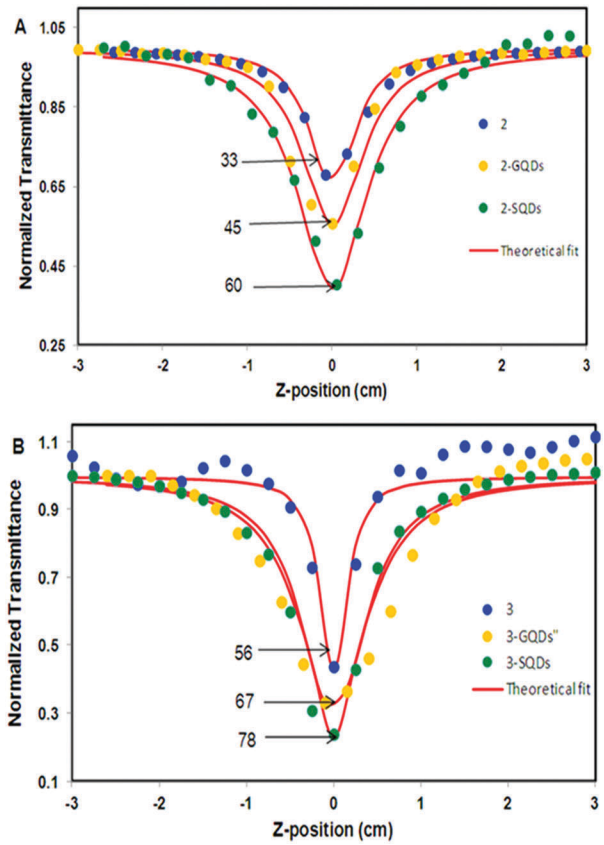

Fig. 6 Open-aperture Z-scans and percentage linear transmittance for complexes **2** and **3** and their nanoconjugates in DMSO. Filled circles represent experimental data while the solid lines are theoretical fits.

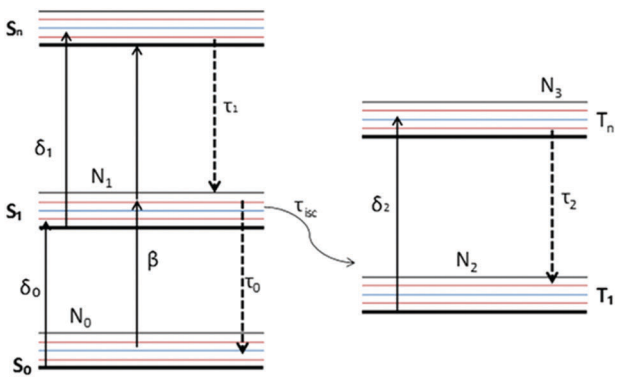

Fig. 7 Five level energy diagram explaining the dynamics of the excited state population (solid arrows) and non-radiative relaxation (dashed arrows) in the studied complexes.

the fluorescence lifetime (τ_F) and triplet quantum yield (Φ_T) using the relationship (τ_F/Φ_T) and were in the nanosecond time scale, Table 1. Since the observed triplet lifetime is far longer than the intersystem crossing lifetime, the rate of intersystem crossing to populate the triplet state will be high resulting in high population build up in the triplet state. Molecules from the T_1 state can be further excited to the T_n state with absorption cross-section δ_2.

These transitions can be treated with the 5-level model rate eqn (10)–(13):

$$\frac{\partial N_1}{\partial t} = -\frac{\partial_0 I N_0}{h\omega} - \frac{\beta I^2}{2h\omega} + \frac{N_0}{\tau_0} + \frac{N_2}{\tau_1} \quad (10)$$

$$\frac{dN_2}{dt} = \frac{\delta_1 I N_1}{\hbar\omega} + \frac{\beta I^2}{2\hbar\omega} - \frac{N_1}{\tau_1} \quad (11)$$

$$\frac{dN_3}{dt} = -\frac{\delta_2 I N_3}{\hbar\omega} - \frac{N_2}{\tau_2} + \frac{N_0}{\tau_{isc}} + \frac{N_3}{\tau_3} \quad (12)$$

$$\frac{dN_3}{dt} = -\frac{\delta_2 I N_3}{\hbar\omega} - \frac{N_2}{\tau_2} + \frac{N_0}{\tau_{isc}} + \frac{N_3}{\tau_3} \quad (13)$$

where δ_0, δ_1 and δ_2 are the ground, singlet and triplet excited state absorption cross sections, respectively, $\hbar$ is Planck's constant, ω is the frequency of light, the N_i values represent the populations in the different states, β is the two photon absorption (TPA) cross-section, the τ_i values are the lifetimes of the excited states and τ_{isc} is the lifetime of intersystem crossing.

The intensity transmitted through the sample is represented as I, given by eqn (14)–(16).

$$\frac{dI}{dt} = \frac{c}{n_r}\frac{dI}{dz} = \frac{cI}{n_r}[\delta_0 N_1 + \delta_1 N_2 + \delta_2 N_3] \quad (14)$$

$$I = I_{00}\left(\frac{\omega_0^2}{\omega^2(z)}\right)\exp\left(-\frac{t^2}{\tau_p^2}\right)\exp\left(-\frac{2r^2}{\omega^2(z)}\right) \quad (15)$$

$$\omega(z) = \omega_0\sqrt{\left\{1 + \left(\frac{z}{z_0}\right)^2\right\}};\quad z_0 = \frac{\pi\omega_0^2}{\lambda} \quad (16)$$

where n_r is the refractive index (n_r = 1.479 in DMSO), c is the speed of light in a vacuum, I_{00} is the peak intensity at the focus of a Guassian beam, τ_p is the input pulse width at time t, ω_0 is the beam waist at focus, z_0 is Rayleigh range, λ is the wavelength of the laser and r is the radius of the aperture. dI/dz in eqn (14) describes the change of photon flux with propagation of laser light through the sample with z as the position of the sample in the beam profile.

Since the nanosecond laser pulse used in this study is far longer than the femtosecond lifetimes of the S_n and T_n states,[48–50] these levels can be neglected, and only the time variation of populations N_0, N_1 and N_2 for the S_0, S_1 and T_1 energy levels are included in eqn (10)–(13). The rate equations were numerically solved following the methods of Zhang *et al.*[51]

It can be observed that the theoretical fitting from the model (solid lines) is well fitted to the experimental data (scattered point) (Fig. 6A and B). The ground state absorption cross-section was obtained from absorption spectroscopy using eqn (17)

$$\delta_0 = \alpha/N_0 \quad (17)$$

where α is the linear absorption and N_0 is the number of molecules per cm^3.

The absorption cross-sections found through the fitting for δ_1 range from 1.02×10^{-17} cm^2 to 93.80×10^{-17} cm^2 (4–25 times higher than δ_0). The absorption cross-sections due to triplet (δ_2) range from 1.8×10^{-17} cm^2 to 153×10^{-17} cm^2 (7–19 times higher than the δ_0) (Table 3). The contribution due to TPA ranges from 172 GM to 343 GM (1 GM = 10–50 cm^4 s $photon^{-1}$). These values are close to those reported in the literature for phthalocyanines using nanosecond pulse duration.[52,53] It can be clearly seen that the singlet and triplet contributions dominate the observed RSA Z-scan profile. This is expected since Pcs are known to exhibit RSA at higher fluence and nanosecond pulse durations due to strong absorption in the triplet manifold.[53] This can be explained since the intersystem crossing in Pcs usually occurs within a nanosecond time frame, while the triplet state has longer lifetimes in the microsecond scale,[52,54] hence rapid intersystem crossing populates the triplet excited state, which is further enhanced due to the presence of heavy atoms. The semiconductor quantum dot conjugates showed an enhanced triplet population compared to the corresponding graphene quantum dot conjugates, which can be attributed to the above mentioned heavy atom effect. The higher TPA in **2**-SQDs, **3**-SQDs, and **4**-SQDs compared to the corresponding **2**-GQDs, **3**-GQDs and **4**-GQDs, could be explained because the absorption wavelength of the SQDs is resonant with the excitation wavelength of the laser. Apart from this, the free carrier absorption in semiconductor quantum dots, which involve electron excitation from the valence band to the conduction band favors the TPA pathway.[55]

Table 3 Nonlinear optical parameters of the complexes and nanoconjugates in DMSO

Sample	β (GM)	δ_0 (cm^2) 10^{-18}	δ_1 (cm^2) 10^{-17}	δ_2 (cm^2) 10^{-16}	δ_1/δ_0	δ_2/δ_0	I_{lim}
2	245	2.37	1.02	1.80	4.3	7.59	—
3	207	2.95	6.37	5.00	21.59	16.94	1.23
4	204	81.00	89.5	11.01	11.04	13.60	1.08
2-GQDs	186	2.37	2.47	2.80	10.42	11.81	—
2-SQDs	288	2.41	3.15	4.00	13.07	16.60	1.43
3-GQDs	202	2.88	4.23	5.10	17.71	17.71	0.67
3-SQDs	317	3.90	3.11	10.10	25.90	25.90	0.42
4-GQDs	172	81.0	93.8	103.0	12.63	12.63	0.48
4-SQDs	343	81.0	86.5	153.0	18.89	18.89	0.32

One prerequisite property of an ideal optical limiter is exhibition of a linear transmittance below the threshold, but clamp out the output fluence to a constant value at a critical intensity, thus providing safety to sensors including the human eye. Materials with this property are desirable in a variety of circumstances where a decreasing transmission with increasing excitation is desired such as in laser pulse shaping applications. The limiting threshold (I_{lim}) can be defined as the input fluence at which the transmittance is 50% of the linear transmittance.[56] The lower the I_{lim} value, the better the material as an optical limiter.

The limiting thresholds for the complexes and the nanoconjugates were determined using the plot of transmittance against input fluence (Fig. S11, ESI†). The I_{lim} values of **2** and **2**-GQDs could not be determined since the transmittance did not drop below 50% (Table 3 and Fig. S11, ESI†).

The I_{lim} values for complex **4** were found to be 1.08 J cm^{-2}, lower than that of complex **3** due to the heavy atom effect of indium (in complex **4**) compared to gallium (in complex **3**) (Table 3). Lower I_{lim} values were observed when the complexes

were covalently linked to QDs with SQDs conjugates showing a lower limiting threshold than the corresponding GQDs conjugates. It is noteworthy that the complexes reported in this work showed a lower limiting threshold, and therefore a superior nonlinear optical response compared to monomeric analogues reported in the literature,[57] suggesting that dimerization could be a potential means of tuning NLO responses in materials.

Conclusions

The photo-induced resonance energy transfer and nonlinear optical response of carboxylic acid substituted ball-type phthalocyanines in solution and when covalently linked to quantum dots are reported. The efficiency of energy transfer was observed to be higher when the complexes were linked with semiconductor quantum dots than when linked with graphene quantum dots. The open aperture Z-scan technique at 532 nm and 10 ns pulse was used to probe the nonlinear optical performance of the studied complexes. The results of the nonlinear optical study showed that both the complexes consistently exhibit RSA behavior in solution and when conjugated to QDs. The observed RSA behaviour was found to be dominated by excited state absorption in the singlet and triplet manifolds.

Conflicts of interest

There are no conflicts to declare.

Acknowledgements

The authors acknowledge Technology (DST) and National Research Foundation (NRF) of South Africa through DST/NRF South African Research Chairs Initiative for Professor of Medicinal Chemistry and Nanotechnology (UID 62620), and Rhodes University.

References

1 A. Tuhl, H. Manaa, S. Makhseed, N. Al-Awadi, J. Mathew, H. M. Ibrahim, T. Nyokong and H. Behbehani, *Opt. Mater.*, 2012, **34**, 1869–1877.
2 E. M. García-Frutos, S. M. O'Flaherty, E. M. Maya, G. de la Torre, W. Blau, P. Vázquez and T. Torres, *J. Mater. Chem.*, 2003, **13**, 749–753.
3 Y. Chen, L. Gao, M. Feng, L. Gu, N. He, J. Wang, Y. Araki, W. J. Blau and O. Ito, *Mini-Rev. Org. Chem.*, 2009, **6**, 55–65.
4 G. de la Torre, P. Vázquez, F. Agulló-López and T. Torres, *J. Mater. Chem.*, 1998, **8**, 1671–1683.
5 Y. Gao, N. Q. Huong, J. L. Birman and M. J. Potasek, *J. Appl. Phys.*, 2004, **96**, 4839–4842.
6 R. A. Ganeev, A. I. Ryasnyansky, S. R. Kamalov, M. K. Kodirov and T. Usmanov, *J. Phys. D: Appl. Phys.*, 2001, **34**, 1602–1611.
7 X. Wu Chen, X. Sun, J. Lin, W. Ji and K. Tan, *Phys. Rev. Lett.*, 1999, **82**, 2548–2551.
8 L. Pan, N. Tamai, K. Kamada and S. Deki, *Appl. Phys. Lett.*, 2007, **91**, 1–4.
9 A. A. Umar, A. H. Reshak, M. Oyama and K. J. Plucinski, *J. Mater. Sci.: Mater. Electron.*, 2012, **23**, 546–550.
10 I. Dancus, V. I. Vlad, A. Petris, N. Gaponik, V. Lesnyak and A. Eychmüller, *Opt. Lett.*, 2010, **35**, 1079–1081.
11 A. Wang, L. Long, W. Zhao, Y. Song, M. G. Humphrey, M. P. Cifuentes, X. Wu, Y. Fu, D. Zhang, X. Li and C. Zhang, *Carbon*, 2013, **53**, 327–338.
12 D. A. Wheeler and J. Z. Zhang, *Adv. Mater.*, 2013, **25**, 2878–2896.
13 S. Sadhu, K. K. Haldar and A. Patra, *J. Phys. Chem. C*, 2010, **114**, 3891–3897.
14 A. Rakovich, I. Nabiev, A. Sukhanova, V. Lesnyak, N. Gaponik, Y. P. Rakovich and J. F. Donegan, *ACS Nano*, 2013, **7**, 2154–2160.
15 J. Britton, C. Litwinski, M. Durmuş, V. Chauke and T. Nyokong, *J. Porphyrins phthalocyanines*, 2011, **15**, 1239–1249.
16 Z. B. Liu, Y. F. Xu, X. Y. Zhang, X. L. Zhang, Y. S. Chen and J. G. Tian, *J. Phys. Chem. B*, 2009, **113**, 9681–9686.
17 M. B. M. Krishna, N. Venkatramaiah, R. Venkatesan and D. N. Rao, *J. Mater. Chem.*, 2012, **22**, 3059–3068.
18 N. Nwaji, D. O. Oluwole, J. Mack, M. Louzada, S. Khene, J. Britton and T. Nyokong, *Dyes Pigm.*, 2017, **140**, 417–430.
19 M. Xue, X. Wang, H. Wang and B. Tang, *Talanta*, 2011, **83**, 1680.
20 O. J. Achadu, I. Uddin and T. Nyokong, *J. Photochem. Photobiol., A*, 2016, **324**, 96–105.
21 S. Fery-Forgues and D. Lavabre, *J. Chem. Educ.*, 1999, **76**, 1260–1264.
22 A. Ogunsipe, J. Chen and T. Nyokong, *New J. Chem.*, 2004, **28**, 822–827.
23 T. Nyokong and E. Antunes, in *The handbook of porphyrin science*, ed. K. M. Kadish, R. M. Smith and R. Guilard, World Scientific, Singapore, 2010, vol. 7.
24 R. F. Kubin and A. N. Fletcher, *J. Lumin.*, 1982, **27**, 455–462.
25 N. Srinicasan, C. A. Haney, J. S. Lindsey, W. Zhang and B. T. Chait, *J. Porphyrins phthalocyanines*, 1999, **32**, 283–291.
26 M. J. Stillman and T. Nyokong, in *Phthalocyanines. Principles and properties*, ed. C. C. Leznoff and A. B. P. Lever, New York, 2003, vol. 1.
27 E. Gurel, M. Pişkin, S. Altun, Z. Odaba and M. Durmuş, *Dalton Trans.*, 2015, **44**, 6202–6211.
28 Z. Odabas, F. Dumludag, A. R. Ozkaya, S. Yamauchi, N. Kobayashi and Ö. Bekaroğlu, *Dalton Trans.*, 2010, **39**, 8143–8152.
29 Z. Odabaş, I. Koç, A. Altindal, A. R. Özkaya, B. Salih and Ö. Bekaroğlu, *Synth. Met.*, 2010, **160**, 967–977.
30 J. Kleinwächter and M. Hanack, *J. Am. Chem. Soc.*, 1997, **119**, 10684–10695.
31 M. Canlıca, A. Altındal and T. Nyokong, *J. Porphyrins phthalocyanines*, 2012, **16**, 826–832.
32 L. Li, J. Zhao, N. Won, H. Jin, S. Kim and J. Chen, *Nanoscale Res. Lett.*, 2012, **7**, 386–393.
33 Z. Chai, Y. Gao, D. Kong and W. Wu, *J. Nanomater.*, 2016, 9138059.
34 D. Cotter, M. G. Burt and R. J. Manning, *Phys. Rev. Lett.*, 1992, **68**, 1200–1203.
35 J. W. Haus, in *Fundamentals and Applications of Nanophotonics*, ed. J. W. Haus, Woodhead Publishing Series in Electronic and Optical Materials, New York, 2016.
36 C. Vatankhah and A. Ebadi, *Res. J. Recent Sci.*, 2013, **2**, 21–24.
37 P. Recher and B. Trauzettel, *Nanotechnology*, 2010, **21**, 302001.

38 V. G. Kozlov, V. Bulović, P. E. Burrows and S. R. Forrest, *Nature*, 1997, **389**, 362–364.
39 J. R. Lakowicz, *Principles of Fluorescence Spectroscopy*, Springer, 3rd edn, 2006.
40 H. Du, R.-C. A. Fuh, J. Li, L. A. Corkan and J. S. Lindsey, *Photochem. Photobiol.*, 1998, **68**, 141–142.
41 M. G. Debacker, D. Deleplanque, B. V. Vlierberge and F. X. Sauvage, *Laser Chem.*, 1988, **8**, 1–11.
42 R. J. Magyar and S. Tretiak, *J. Chem. Theory Comput.*, 2007, **3**, 976–987.
43 S. Venugopal Rao, P. T. Anusha, L. Giribabu and S. P. Tewari, *Pramana*, 2010, **75**, 1017–1023.
44 M. Hanack, T. Schneider, M. Barthel, J. S. Shirk, S. R. Flom and R. G. S. Pong, *Coord. Chem. Rev.*, 2001, **219–221**, 235–258.
45 N. K. M. N. Srinivas, S. V. Rao and D. N. Rao, *J. Opt. Soc. Am. B*, 2003, **20**, 2470.
46 T.-H. Wei, T.-H. Huang and T.-C. Wen, *Chem. Phys. Lett.*, 1999, **314**, 403–410.
47 S. V. Rao, D. N. Rao, J. A. Akkara, B. S. DeCristofano and D. V. G. L. N. Rao, *Chem. Phys. Lett.*, 1998, **297**, 491–498.
48 A. W. Snow, J. R. Griffith and N. P. Marullo, *Macromolecules*, 1984, **17**, 1614–1624.
49 K. S. Lee and M. A. El-Sayed, *J. Phys. Chem. B*, 2006, **110**, 19220–19225.
50 P. K. Jain, K. S. Lee, I. H. El-Sayed and M. A. El-Sayed, *J. Phys. Chem. B*, 2006, **110**, 7238–7248.
51 C. Zhang, Y. Wang, J. Zhao, Q. Gary and G. M. Lawson, Optical Society of America, 2015, paper NW4A.23.
52 D. S. Chemla and J. Zyss, *Nonlinear Optical Properties of Organic Molecules and Crystals*, Academic Press, 1987, pp. 1–482.
53 A. B. Karpo, V. E. Pushkarev, V. I. Krasovskii and L. G. Tomilova, *Chem. Phys. Lett.*, 2012, **554**, 155–158.
54 J. S. Shirk, R. G. S. Pong, F. J. Bartoli and A. W. Snow, *Appl. Phys. Lett.*, 1993, **63**, 1880–1882.
55 V. Sreeramulu, K. K. Haldar, A. Patra and D. N. Rao, *J. Phys. Chem. C*, 2014, **118**, 30333–30341.
56 Y. Chen, M. Hanack, W. J. Blau, D. Dini, Y. Liu, Y. Lin and J. Bai, *J. Mater. Sci.*, 2006, **41**, 2169–2185.
57 D. O. Oluwole, S. M. Ngxeke, J. Britton and T. Nyokong, *J. Photochem. Photobiol., A*, 2016, **347**, 146–159.

